Recycling of Expired drug (levofloxacin hemihydrate) as a potential Eco-friendly Inhibitor for Copper in Synthetic Acid Rain Solution (SAR)

Atiat A. Montaser[1*], Mohamed Sarwat El-Mahdy[1], Elsayed E. E. Mahmoud[1], A. S. Fouda[2*]

[1]Department of Chemistry, Faculty of Science, Aswan University, Aswan 81528, Egypt.

[2]Department of Chemistry, Faculty of Science, Mansoura University, Mansoura 35516, Egypt.

Abstract:

This study focused on the recycling of the expired Levofloxacin hemihydrate (LFH) for preventing copper (Cu) corrosion caused by synthetic acid rain (SAR) solution employing electrochemical techniques potentiodynamic polarization (Tafel Polarization) and electrochemical impedance spectroscopy (EIS); and chemical method (weight loss (WL)). Results showed that LFH is an efficient inhibitor for copper corrosion, and the inhibition efficiency percent (η%) reached 88.4 % at an optimum concentration (600 ppm) according to EIS measurements. The data of WL method revealed that the inhibition efficiency (η%) raised and the corrosion rate (k_{corr}) decreased with the concentration of LFH and vice versa with the temperature. It was discovered that the adsorption of the LFH on the Cu surface obeyed Langmuir adsorption isotherm. The Tafel curves demonstrated that this expired behaved as a mixed-type inhibitor. The LHF prevented corrosion by adhering to the metal surface, which was demonstrated by Scanning Electron Microscopy Conducted with Energy Dispersive X-ray (SEM-EDX), Atomic Force Microscopy (AFM), and Fourier Transform Infrared Spectroscopy (FT-IR).

1- Introduction

The recovery of active ingredients in pharmaceuticals that are now present in greater quantities, both in homes and pharmacies, hospitals, etc., poses a new issue as a result of the usage of expired medications as corrosion inhibitors for various metals and alloys in recent years. Large molecules with hetero atoms like nitrogen, sulfur, oxygen, and π bonding in their structures are characteristics that suggest the usage of active ingredients from expired medications in the prevention of corrosion (Singh et al., 2017).

Additionally, the majority of these chemicals have high water solubility and are stable in a variety of hostile conditions. More than 88% of medications reportedly include active components that maintain their stability and don't deteriorate over time after their expiration date (Lyon et al., 2006).

Corresponding author*: E-mail address: atiat70@yahoo.com; asfouda@mans.edu.eg

According to the previously discussed factors, it is safe to use expired medications. Additionally, due to their non-toxicity and minimal influence on the environment, these commercially available pharmaceuticals appear to have the potential to replace conventional poisonous chemical corrosion inhibitors (Singh et al., 2017). The expired medications belonged to the same class as the green corrosion inhibitors, as well. With an increase in the amount of expired medications, their usage as corrosion inhibitors may reduce environmental pollutants in addition to lowering the expenses associated with the disposal and degradation of these expired medications (Fouda et al., 2022; Montaser et al., 2023).

Due to its exceptional mechanical and thermal conductivity, copper is a metal with many uses. It is employed in electronics, the manufacture of cables, tubes, and sheets, as well as the creation of metal alloys (Dueke Eze et al., 2022; El Ibrahimi, 2021). A relatively noble metal is copper. However, in typical, oxygen-containing conditions, it responds quickly. The consequences of significant worldwide environmental issues and the deterioration of outdoor structures due to acid rain have emerged as pressing concerns. The effective management of corrosion is of paramount importance in terms of its practicality and applicability (Al Kharafi et al., 2010; Zhang et al., 2019).

Numerous researchers have been interested in the potential for Cu corrosion prevention in different aqueous solutions; therefore, up till now, several potential inhibitors have been investigated. Corrosion protection can be distinguished by compounds that are added to the environment in minute amounts to prevent additional metal disintegration.

According to Fateh et al. (2020) several corrosion inhibitors can be used to safeguard copper. Many recent works have discussed the use of the antibiotics norfloxacin, cefadroxil, ofloxacin, and tacrine to prevent corrosion in metals (Montaser et al., 2023; Thanapackiam et al., 2017; Thanapackiama et al., 2019; Yao et al., 2019).

The pharmaceutical LFH is a form of Levofloxacin containing water molecules in its crystal structure. The existence of molecules of water changes the physical properties of the medication, such as solubility, which can affect its absorption and efficiency. Because the pharmaceutical LFH compound contains O, N, and F atoms, enables it to bind to metal surfaces. It is the first time to use the expired LFH as a corrosion inhibitor for Cu in this study, but the use of the mother compound (Levofloxacin) was mentioned in Table 1.

This paper reports the expired LFH's efficiency as a sustainable inhibitor for Cu corrosion in SAR solution, using a combination of chemical and electrochemical techniques as well as surface characterization by SEM-EDX, AFM, and FTIR analysis.

Table 1. A list of LFH utilized in preventing metal corrosion in an acidic environment.

Metal or alloy	Media	η%	year	Ref.
Mild Steel	0.5 M H_2SO_4	87.8	2011	(Pang et al., 2011)
Carbon Steel	2 M HCl	88.35	2017	(Ikpi et al., 2017a)
API 5L X-52 steel	2 M HCl	91.3	2017	(Ikpi et al., 2017b)
Cast Iron	1 M HCl	93.4	2017	(Rajeswari et al., 2017)
AA2024-T4	3.5% NaCl	86	2019	(Zheng et al., 2020)
Copper	Synthetic Acid Rain solution	88.4	------	Present study as LFH

2. Materials and Methods

2.1 Materials

In this research, the chemical composition of Cu is Si (0.25 %), Fe (0.09%), and the remainder of the weight percentage is Cu. The specimens were mechanically cut into about 8–9 cm^2 for Mass loss and 1 cm^2 for electrochemical measurement techniques. These samples were polished, then rinsed with bidistilled water, dried, and preserved in a dissector as described elsewhere (Montaser et al., 2023).

2.2 Chemicals and Solutions

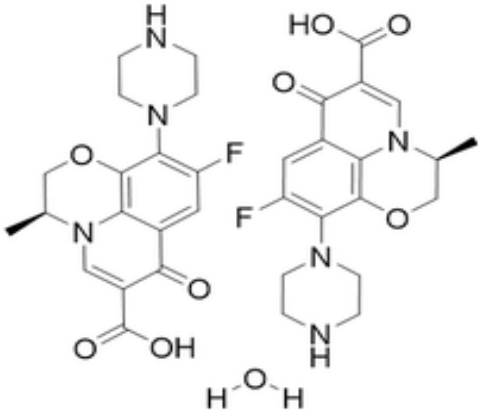### 2.2.1 Preparation of Synthetic Acid Rain Solution (SAR)

The corrosive working solution (SAR) was prepared from the following ingredients $NaNO_3$ (0.2 g/L), $NaHCO_3$ (0.2 g/L), and Na_2SO_4 (0.2 g/L) using bidistilled water (Razli et al., 2011). To get the pH value 2.42, 0.1 N H_2SO_4 solution was used (Tasić et al., 2019). All materials utilized in the study were of an AR-grade and were applied in accordance with their original specifications.

2.2.2 Separation of the Active Substance of the Drug and Preparation Inhibitor Concentrations.

The LFH was obtained as expired tablets and dissolved in SAR solution after a special separation technique from their Inactive ingredients (coating materials). The tablet's FTIR spectra are first performed to provide mixing spectra for the drug and inactive ingredients. According to the drug's label, may be some or a mix of insoluble starch, microcrystalline cellulose, lactose monohydrate, ferric oxide, magnesium stearate, croscarmellose sodium, Hypromellose, titanium dioxide, and polyethylene glycol. The tablet is then dissolved in SAR solution and filtered using a vacuum pump and filter paper with a 0.45 μm porosity.

The stock solution of LFH (1000 ppm) was used to prepare the wanted doses by diluting them with bi-distilled water. The concentration of LHF utilized was 100-600 ppm. The structure of LFH is shown in Table 2.

Table 2. Structure details of LFH

Mol. Formula	Mol. Weight	Molecular structure
$C_{36}H_{42}F_2N_6O_9$	740.7gm	

2.4 Methods

2.4.1 Characterization of LFH

Following the filtration procedures, the precipitate was dried and re-analyzed by the FTIR instrument to produce only the inactive ingredients spectra in order to confirm that the active medication had been entirely dissolved. In order to make sure that pharmaceuticals did not lose

their chemical components throughout the dissolving process, a portion of the filtrated solution was again evaporated using a Rota Vapor device at 313 K, dried, and then analyzed by FTIR. In comparison with their coating materials for drugs and their recorded wavenumber, the FTIR of active substances are displayed in Fig. 1 and Table 3.
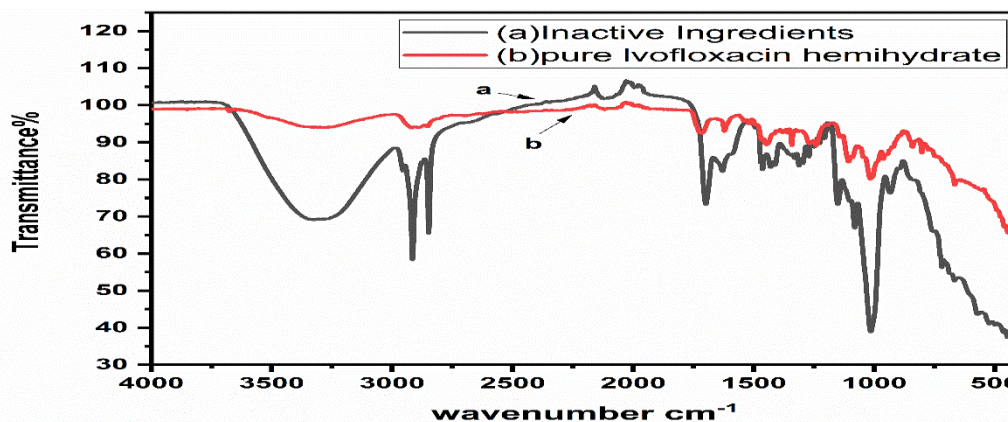

Fig. 1. FTIR of active substance in comparison with their coating materials for LFH.

Table 3 Wavenumber in pure LFH in comparison with their coating materials.

Function group	Wavenumber of pure Levofloxacin hemihydrate, cm^{-1}	Wavenumber of coating materials, cm^{-1}
O–H stretching	3360.5	3301.1
Stretching of C-H bonds	2916.5	2915
The aromatic ring's C-H Stretching	2828	ND
Stretching of C=O in COOH	1715.5	ND
4-quinolone ring stretching C=O	1617.3	ND
The aromatic ring's C=C stretching	1469.9	ND
C–H bending	1449.2	1463.6
C–N stretching	1340.1	ND
C–O stretching in COOH	1267.9	ND
C–O stretching in O-C–O	ND	1151.2
C–F stretching	1106.5	ND

2.4.1 Weight Loss (WL)

The influence of the addition of LFH (100-600 ppm) on Cu corrosion in SAR solution was studied by WL at (298 – 318 K) after 6 hours of immersion. The inhibition efficiency (η%) and degree of surface area coverage (θ) are calculated as follows:

$$\eta\% = (\theta \times 100) \qquad (1)$$

$$\theta = (1 - (\frac{k_{corr}^i}{k^o})) \tag{2}$$

Where k^o and k_{corr}^i are the corrosion rates of Cu without and with LFH, respectively, in (mg cm^{-2} min^{-1}). Using Equation (3), the corrosion rate (k_{corr}) was calculated with regard to weight loss:

$$k_{corr} = \Delta W / A.t \tag{3}$$

where A is the surface area of the Cu samples (cm^2) and Cu's weight loss (mg cm^{-2}) is reported as ΔW during immersion time t (min).

2.4.2 Electrochemical Measurements

Electrochemical measurement experiments were conducted using a conventional three-electrode setup consisting of Ag/AgCl electrode, a Pt sheet as the counter electrode, and a Cu working electrode. In order to acquire steady state open circuit potential (E_{ocp}), the Cu electrodes were immersed in the SAR solution for 30 minutes prior to beginning measurements.

The potentiodynamic polarization curves were scanned from −0.2 V vs. E_{ocp} to +0.2 mV vs. E_{ocp} at a scan rate of 1.0 mV s^{-1}. Polarization curves, both cathodic and anodic, from Cu in SAR solution and Cu in SAR with the inclusion of various LFH concentrations are utilized to identify the current potential characteristics. Corrosion potentials (E_{corr}), corrosion current densities (j_{corr}), anodic and cathodic Tafel slopes (β_a, β_c), as well polarization resistances (Rp) for each experiment, were determined. These data were employed to evaluate the inhibition efficiency (η %) calculated from the values obtained from j_{corr} according to Equation (4):

$$(\eta \%) = (1 - \left(\frac{j_{corr}}{j_{corr}^°}\right)) \times 100 \tag{4}$$

where $j_{corr}^°$ is the corrosion current without LFH and j_{corr} is the corresponding corrosion current with LFH.

In the frequency range of 10^3 Hz to 0.01 Hz, impedance measurements (EIS) were performed at open circuit potential (E_{ocp}) with an AC voltage amplitude of 10 mV. By adjusting the model to the experimental data, the impedance parameters were determined to the equivalent circuit model in ZSimpWin software.

Accordingly, the efficiency of LFH as an inhibitor was then determined using Equation (5):

$$(\eta\%) = (\theta \times 100) = (1 - (\frac{R_{ct}^°}{R_{ct}})) \times 100 \tag{5}$$

where $R_{ct}^°$ and R_{ct} are the charge transfer resistance without and with varying LFH concentrations in the SAR solution, respectively.

For each experiment, a VersaSTAT4 potentiostat/Galvanostat was coupled to a laptop at 298 K in the absence or in the presence of LFH at concentrations ranging from 100 to 600 ppm.

2.4.3 Surface Morphology

Copper samples were analyzed by SEM-EDX (JSM-IT200) and AFM (PicoSPM-2100) to determine the morphology of their surfaces while in SAR solution with and without the appropriate concentration of the inhibitors.

2.4.4 Fourier-Transform Infrared Spectroscopy (FTIR) Analysis.

On a Shimadzu FTIR Tracer-100, FT-IR spectra were obtained from a purified solution of LFH and whereby Cu sheets were subjected to SAR + 600 ppm of LFH drug for 6 hours.

3. Results and Discussion
3.1. Chemical Measurements
3.1.1 WL Measurements and Temperature Effect

ML was carried out in SAR solution for Cu at different LFH concentrations at 298- 318 K. Fig. 2. shows that increasing the concentration of LFH lowers the corrosion rate and therefore increases inhibition efficiency. Corrosion rates (k_{corr}) and the corresponding inhibition efficiencies ($\eta\%$) for Cu in SAR with varied dosages of inhibitor at given temperatures are displayed in Fig. 3. k_{corr} is extremely reduced in the presence of LFH which exhibits temperature- and concentration-dependent. Obviously, increasing the drug's concentration lowers k_{corr} value at a constant temperature; this is due to the adsorption of LFH molecules creating a protective layer on the Cu surface, suppressing the interaction of the metal surface with acidic media (Fouda et al., 2023). While raising the temperature accelerates copper dissolution in SAR at a subjective dosage of inhibitor, this is because raising the temperature drops the inhibitive efficacy of the drug for the aggravated thermal motion of corrosive species at the copper/SAR interface. Besides, high temperature weakens the viscosity of the adsorbed layer and hence causes the lowering $\eta\%$ (Fan et al., 2020).
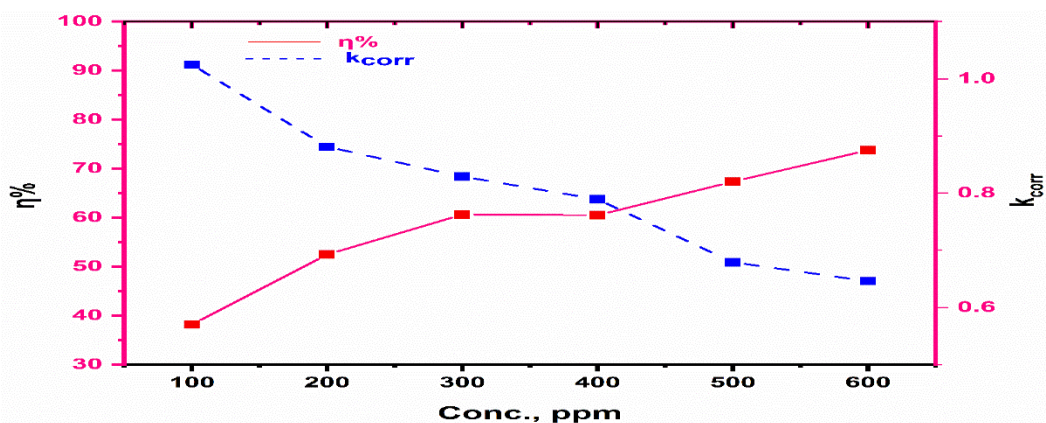

Fig. 2. Influence of LFH concentration on the effectiveness of inhibition and corrosion rate (k_{corr}) of Cu in SAR at 298K.
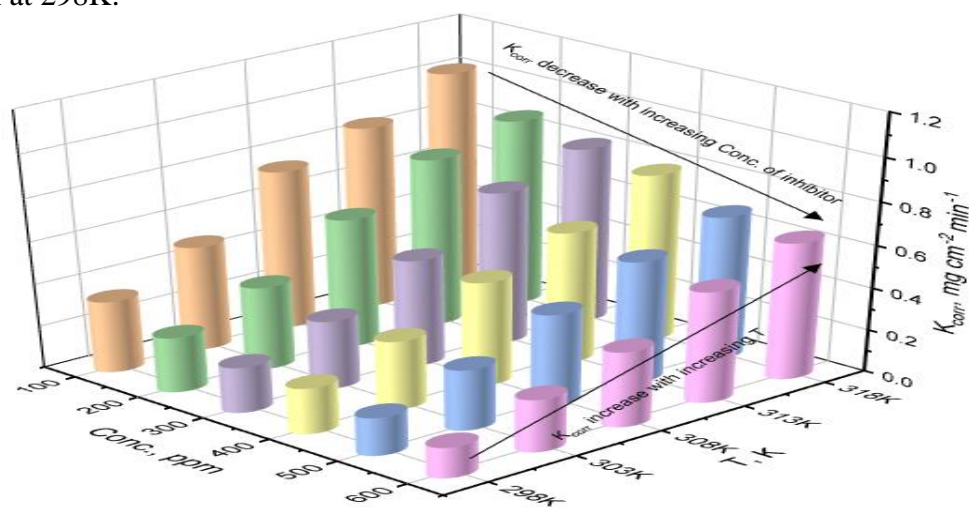

Fig. 3. Influence of the temperature on Cu's corrosion rate (k_{corr}) in SAR in the presence of varying LFH concentrations.

Table 4 displays the estimated values for corrosion rate (k_{corr}), inhibition efficiency ($\eta\%$), and surface overage (θ).

Table 4. Effect of LFH concentrations on the k_{corr} (mg cm^{-2}min^{-1}) and ($\eta\%$) in SAR solution at different temperatures after an immersion of 6 hours.

Temperature (K)	Conc. (ppm)	$k_{corr} \times 10^{-3}$ (mg cm^{-2}min^{-1})	η %	θ
	BLANK	0.55		
	100	0.34	38.17	0.38
	200	0.26	52.46	0.52
298	300	0.22	60.62	0.61
	400	0.22	60.48	0.60
	500	0.18	67.34	0.67
	600	0.14	73.74	0.74
	BLANK	0.71		
	100	0.49	30.51	0.31
	200	0.39	44.90	0.45
303	300	0.32	54.35	0.54
	400	0.32	54.35	0.54
	500	0.29	59.62	0.60
	600	0.25	65.10	0.65
	BLANK	1.02		
	100	0.75	26.32	0.26
	200	0.61	40.13	0.40
308	300	0.50	50.46	0.50
	400	0.49	51.71	0.52
	500	0.43	57.39	0.57
	600	0.36	65.12	0.65
	BLANK	1.17		
	100	0.86	26.71	0.27
	200	0.79	32.50	0.32
313	300	0.72	38.63	0.39
	400	0.62	47.22	0.47
	500	0.57	51.15	0.51
	600	0.52	55.33	0.55
	BLANK	1.33		
	100	1.02	23.13	0.23
	200	0.88	33.91	0.34
318	300	0.83	37.82	0.38
	400	0.79	40.80	0.41
	500	0.68	49.06	0.49
	600	0.65	51.54	0.52

3.1.2 Kinetic-thermodynamic parameters

Arrhenius Equation (6), can be utilized to measure the activation energy for the corrosion reaction (E_a^*)

$$\log A = \frac{E_a^*}{2.303RT} + \log k_{corr} \qquad (6)$$

From Fig. 4, E_a^* can be calculated (Table 5). It was obvious that a significant increase in E_a^* values with the dose of LFH indicating that increased LFH concentrations successfully limit

corrosion by elevating the activation complex's energy barrier, allowing diffusion to take control of the process (Al-Bayaty et al., 2020; Kuraimid et al., 2023).
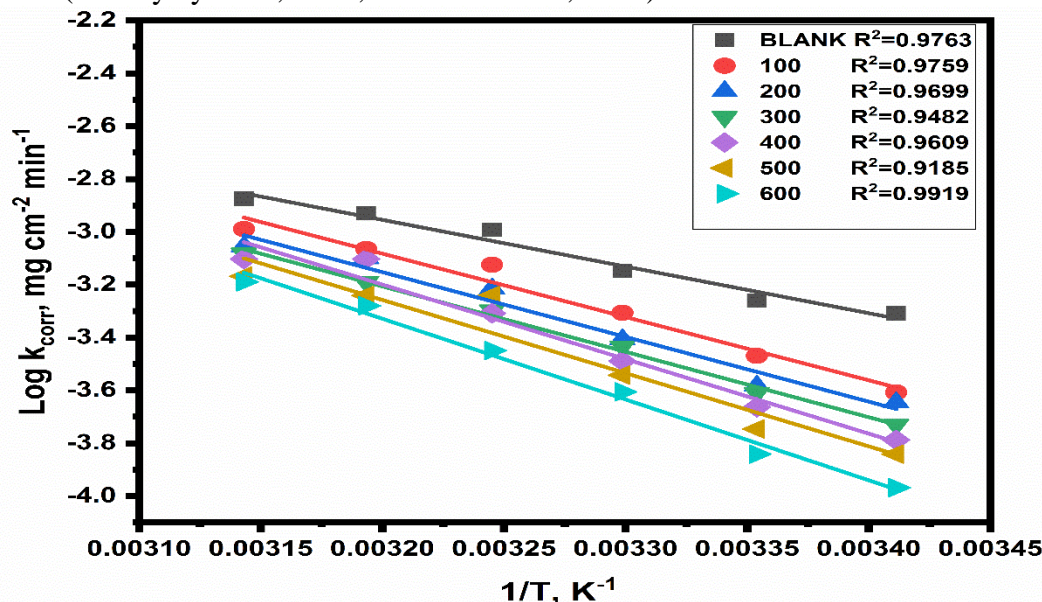

Fig. 4. log (k_{corr}) vs. 1/T with regard to Cu corrosion in SAR solution at different temperatures and variable of LFH concentrations

Table 5. Variables of activation thermodynamics regarding Cu corrosion within SAR solution with and without a range of LFH concentrations.

Activation parameters			
Conc. (ppm)	E_a^* (kJ/mol)	ΔH^* (kJ/mol)	$-\Delta S^*$ (J/mol. K)
Blank	33.83	31.29	550.44
100	45.91	43.37	451.65
200	46.93	44.39	446.44
300	47.68	45.14	445.07
400	54.03	51.47	416.60
500	53.06	46.38	411.44
600	58.57	56.03	354.03

The activation entropy (ΔS^*) and enthalpy (ΔH^*) for the corrosion reaction were estimated utilizing the Eyring transition state equation:

$$\log\left(\frac{k_{corr}}{T}\right) = \left[\left(log\left(\frac{R}{Nh}\right)\right) + log\left(\frac{\Delta S^*}{2.303R}\right)\right] - \frac{\Delta H^*}{2.303RT} \qquad (7)$$

In the given context, N denotes the Avogadro constant, R is the universal gas constant, T denotes the absolute temperature, and h denotes the Boltzmann constant. The determination of ΔH^* and ΔS^* can be achieved by analyzing the intercept and slope of the log (k_{corr} /T) curves plotted against (1/T), as depicted in Fig.5. Table 5 displays the results of the calculations for ΔH^* and ΔS^*. The inclusion of LFH in the solution resulted in a greater value of ΔH^* compared to the blank solution, indicating greater protection from corrosion. For all concentrations and temperatures, E_a^* followed the same general pattern as ΔH^* (see Fig. 6). Similarly, the drug ΔS^*

values are much larger in the uninhibited system than in the inhibited one, demonstrating that the rate-determining step is the association rather than the dissociation between the reagent and the activated complex (Abd El Rehim et al., 2003), and thus that disorder decreases as it moves from the reagent to the activated complex.
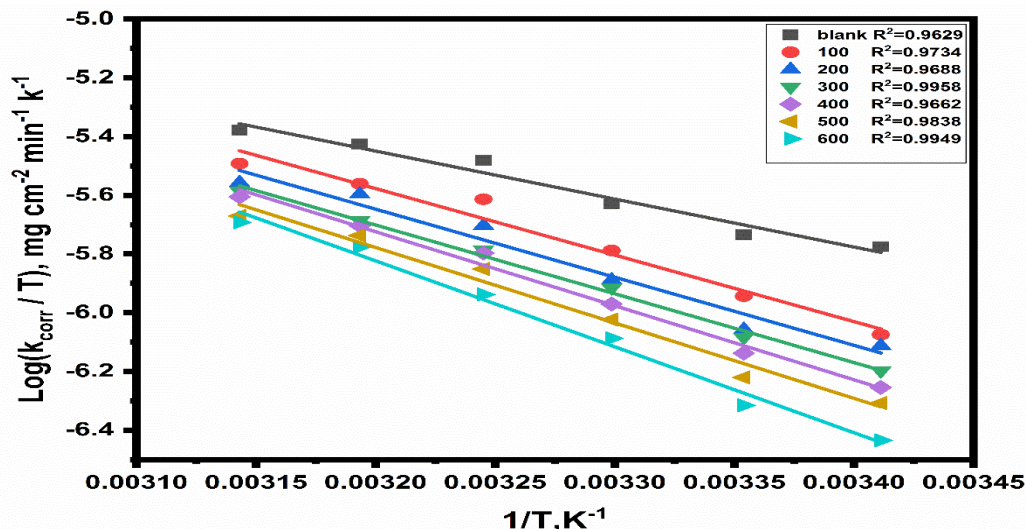

Fig. 5. Plot of Log (k_{corr} /T) versus 1/T plot for Cu corrosion both with and without different LFH concentrations in SAR solution.
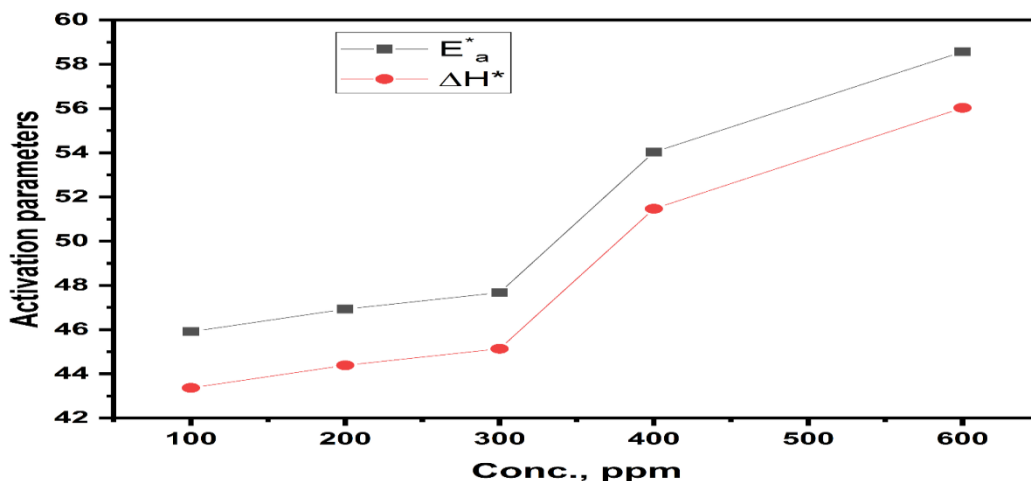

Fig. 6. E_a^* and ΔH^* vs. varying LFH concentrations.

.3.1.3 *Adsorption Isotherm Behavior*

Corrosion protection characteristics have been noted to identify the type of adsorbed inhibitor. A substitutional adsorption process between water molecules on the metallic surface $H_2O_{(ads.)}$ and LFH molecules in the aqueous solution $LFH_{(sol.)}$ can be used to model the adsorption of LFH at the Cu/solution interface (El-Sayed et al., 2023a).

$$LFH_{(sol)} + x\,H_2O_{(ads)} = LFH_{(ads)} + H_2O_{(sol)} \qquad (8)$$

In this equation, x represents the size ratio that indicates how many water molecules are exchanged for one organic adsorbate molecule, where $LFH_{(sol)}$ denotes organic molecules in the

aqueous solution, $LFH_{(ads)}$ denotes organic molecules adsorbed on the Cu surface, and $H_2O_{(ads)}$ denotes water molecules adsorbed on the Cu surface.

Different equations for the adsorption isotherm plots can be obtained if an equilibrium is attained in Equation (8); the extent of surface coverage (θ) for a variety of inhibitor concentrations has been recorded from WL measurements. The values were plots to fit the best isotherm. To define the processes involved in the adsorption of expired LFH, a number of isotherms have been employed, such as the Freundlich, Flory-Huggins, El-Awady, and Langmuir models, on the Cu substrate. using the data's best fit by visualizing (θ) against $\frac{C}{\theta}$ suggesting adsorption of LFH on the Cu surface following Langmuir isotherm model (Fig. 7).

Where, the models of adsorption isotherms are expressed in the following Equations (Farag et al., 2013).

$$\text{Freundlich; } log\ \theta = log\ K_{ads} + n\ log\ C \qquad (9)$$

$$\text{Flory-Huggins; } log\ \left[\frac{\theta}{C}\right]$$
$$= log\ nK_{ads} + n\ log(1 - \theta) \qquad (10)$$

$$\text{El-Awady; } log\ [\frac{\theta}{1 - C}] = logK_{ads} + nlog\ C \qquad (11)$$

$$\text{Langmuir; } \frac{C}{\theta} = \frac{n}{K_{ads.}} + C \qquad (12)$$

Where, the symbol "K_{ads}" represents the equilibrium-adsorption constant, "C" represents the concentration of LFH in parts per million (ppm), "θ" represents the surface coverage, and "*n*" denotes the amount of previously adsorbed water molecules that one inhibitor molecule has replaced.

Gibbs free energy (ΔG°_{ads}) can be determined using equation (13):

$$K_{ads} = (1/999)\ exp\ (\Delta G^{\circ}_{ads} /\ RT) \qquad (13)$$

Where, R represents the gas constant, T denotes the temperature measured in Kelvin, and 999 signifies the concentration of water in the bulk solution expressed in grams per liter. The value of K_{ads} derived from the reciprocal of the intercept of the Langmuir plot lines and the slope of these lines being near unity demonstrates that one metal surface active site is occupied by one inhibitor molecule (Zarrouk et al., 2011).

Thermodynamic parameters derived from the adsorption of the inhibitors on the Cu surface in SAR solution at different temperatures were tabulated in Table 6; since ΔG°_{ads} has a negative sign, and adsorption occurs spontaneously. Adsorption can be classified as either "physical" or "chemisorption" if the ΔG°_{ads} value is less than -20 kJ mol^{-1} or higher than -40 kJ mol^{-1}, respectively (Aribou et al., 2023; Kuraimid et al., 2023). The ΔG°_{ads} data were ranging from 19.96 to 21.68 kJ/mol, showing that mixed adsorption (physical and chemical adsorption) is occurring. The standard enthalpy ΔH°_{ads} and ΔS°_{ads} can be measured using the relation (14):

$$\Delta S^{\circ}_{ads} = \frac{(\Delta H^{\circ}_{ads} - \Delta G^{\circ}_{ads})}{T} \qquad (14)$$

The negative value of ΔH_{ads}° is specified as an exothermic adsorption process (Mu et al., 2005a; Mu et al., 2005b). The negative value of ΔS_{ads}° shows that the LFH particles nitially flowed freely in the bulk solution before settling and becoming adsorbed on the Cu surface, resulting in a negative entropy (Raviprabha et al., 2023).
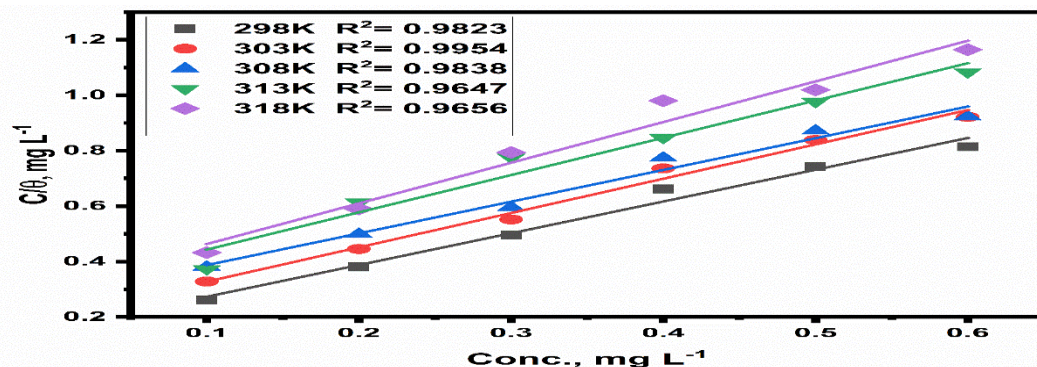

Fig. 7. Cu corrosion Langmuir isotherm fitting in SAR solution with and without various amounts of LFH.

Table 6. Cu corrosion in SAR solution: temperature-dependent adsorption variables.

Temp. (K)	K_{ads} (L/mg)	$-\Delta G_{ads}^{\circ}$ (kJ/mol)	$-\Delta H_{ads}^{\circ}$ (kJ/mol)	$-\Delta S_{ads}^{\circ}$ (J/mol.K)
298	7.20	21.68		
303	6.31	21.06		
308	4.91	20.33	48.56	90.7
313	3.67	20.03		
318	3.24	19.96		

3.2 Electrochemical Measurements

3.2.1 Tafel Measurements

The polarization curve of the Cu electrode in SAR solution containing LFH at 298 K is shown in   Fig. 8. When LFH inhibitor is added to a blank solution, the curve shifts in the direction of reduced current density. The polarization curve's corrosion potential has also been moved negatively, and the cathodic reaction has been inhibited to a greater extent than the anodic reaction (El-Sayed et al., 2023b). This is because the LFH inhibitor creates an adsorption film on the Cu surface, which then serves as a protective layer that primarily prevents copper corrosion by reducing cathode hydrogen and oxygen interactions (El-Sayed et al., 2023b; Xu et al., 2021).

The electrochemical kinetic parameters were estimated using the Tafel extrapolation method to provide a quantitative strategy. These parameters included the corrosion potential (E_{corr}), the cathodic and anodic Tafel slopes (β_c and β_a), the corrosion current density (j_{corr}), the polarisation resistance (R_p), the surface coverage (θ), and the inhibition efficiency ($\eta\%$). Table 7 provides a synopsis of the data collected. Table 7 also displays the inhibition efficiencies ($\eta\%$) determined using Equation (4). According to the data in Table 7, the corrosion current density values drop as LFH concentrations rise.
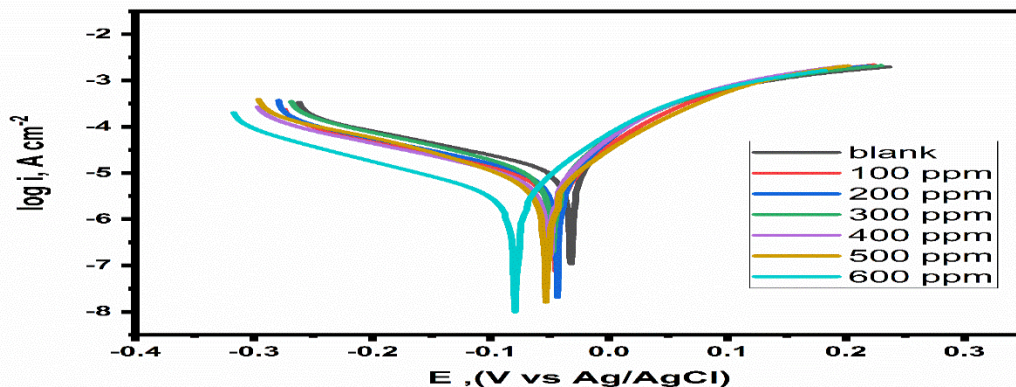
Fig.8. Tafel curves of the dissolution of Cu in different concentrations of LFH in SAR solution at 298 K.

The addition of 600 ppm LFH produced the lowest j_{corr} value, which was almost four times lower than j°_{corr} value estimated for the blank solution. These findings support the LFH drug's ability to prevent copper corrosion in SAR solution. Additionally, within the range of LFH concentrations studied, a change of the E_{corr} values towards more negative values was discernible.

E_{corr} value shifts of less than ±85 mV (El-Sayed et al., 2023a), were interpreted to indicate that the medication under study acts as a mixed-type inhibitor. To the same extent, the addition of LFH to the SAR solution alters the kinetics of both the anodic and cathodic processes as evidenced by variations in the Tafel slopes (Varvara et al., 2022). Besides, the anodic Tafel slope (β_a) values were higher than β_c values; this observation can be understood as a result of the diffusion of corrosion products, which generated on the active sites of anodic sections due to concentration polarization (Deng et al., 2021; El-Sayed et al., 2023b). As inhibitor concentration increases, inhibition efficiency values rise steadily from 41.36 % at 100 ppm LFH to the maximum value of 74.92% achieved with a concentration of 600 ppm LFH.

Table 7. Tafel parameters for Cu without and with different concentrations of LFH in SAR solution at 298 K.

Conc. (ppm)	-E$_{corr}$ mV vs. Ag/AgCl	j$_{corr}$ µA cm^{-2}	β$_a$ mV dec^{-1}	- β$_c$ mV dec^{-1}	R$_P$ kΩ cm^2	θ	η %
Blank	41.40	11.92	200.89	52.7	1.52		
100	42.82	6.99	169.6	55.5	2.60	0.41	41.36
200	45.76	6.9	196.9	54.8	2.70	0.42	42.11
300	47.06	6.51	181	58.8	2.96	0.45	45.39
400	50.81	6.31	175.3	54.8	2.87	0.47	47.06
500	56.07	4.57	175.5	73.6	4.93	0.62	61.66
600	82.45	2.99	175.7	67.2	7.06	0.75	74.92

The percentage of surface porosity was determined using Tafel data. As illustrated below, Stern Geary Equation was applied in order to determine the polarization resistance (El-Sayed et al., 2022).

$$R_P = \frac{\beta}{j_{corr}} \ , \quad \beta = \frac{\beta_a \, \beta_c}{2.303(\beta_a + \beta_c)} \qquad (15)$$

$$P_R = \frac{R_P^o}{R_P} \times 100 \qquad (16)$$

where P_R, corresponds to the total porosity, while R_P^o and R_P are polarization resistance of the uninhibited and inhibited samples of copper, respectively. Fig. 9 depicts the variation in porosity percentage and polarization resistance at 298K due to the presence of LFH. Porosity % dropped drastically when LFH concentration increased. Inhibited copper, then, is more resistant to corrosion than its uninhibited counterpart. This trend is bolstered by the data measured with Tafel plots.
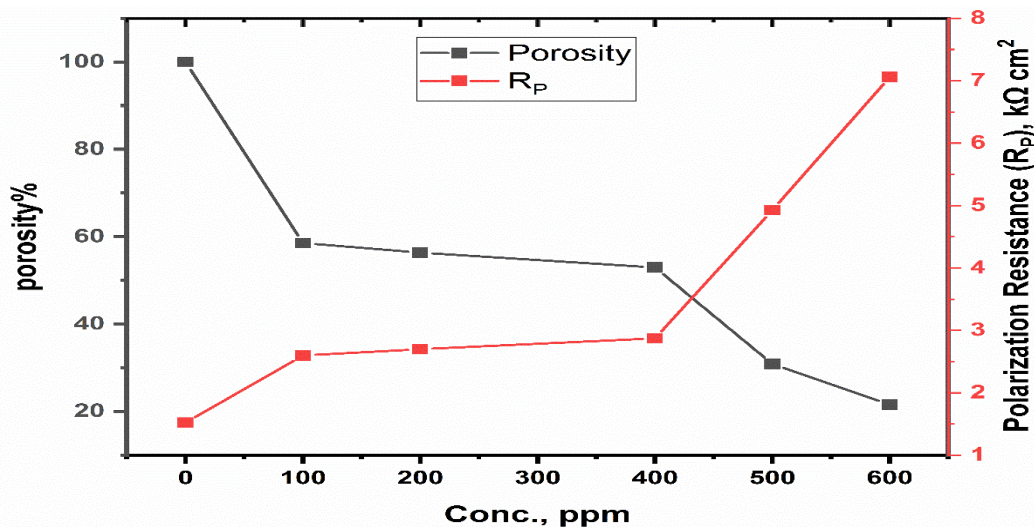

Fig. 9. The Impact of LFH Concentrations on Polarization Resistance and Porosity on Cu corrosion in SAR Solution.

3.2.2 EIS measurements

The impedance diagrams for copper after 30 minutes of immersion in SAR solution are shown in Figs. 10 and 11, both with and without different LFH concentrations. The EIS spectra of the blank solution are easily recognizable by the simple shape of a depressed semicircle followed by a line with an inclination of 45%, which is likely caused by corrosion reactant species diffusing onto the Cu surface (as the development of hydrogen or dissolved oxygen) or species transporting corrosion products (such as soluble cuprous ion complexes) into the solution (Li et al., 2014).

Consequently of the surface's roughness and inhomogeneity, frequency dispersion causes suppressed semicircles (Echihi et al., 2019). Concurrently, when the concentration grows, the diameter of the Nyquist plots expands, signifying that copper is better shielded at greater concentrations (Lamaka et al., 2007). Increased impedance values are proportional to LFH concentrations, as shown by the bode graphs in Fig. 11 along the whole frequency range. For instance, the impendence readings begin to increase until its concentration reaches 600 ppm, suggesting the existence of an effective inhibitor corrosion protection (Lamaka et al., 2007). Additionally, the increased phase angle caused by the rise in LFH concentrations implies greater adsorption of LFH molecules on the Cu surface (Sherif et al., 2008).
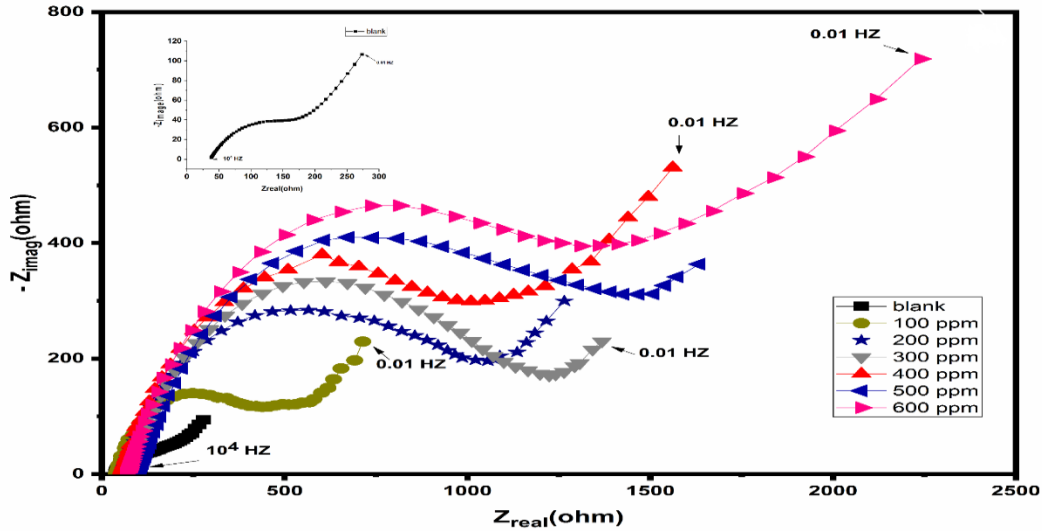
Fig. 10. Nyquist diagrams for Cu in the existence of varying LFH concentrations at 298 K.
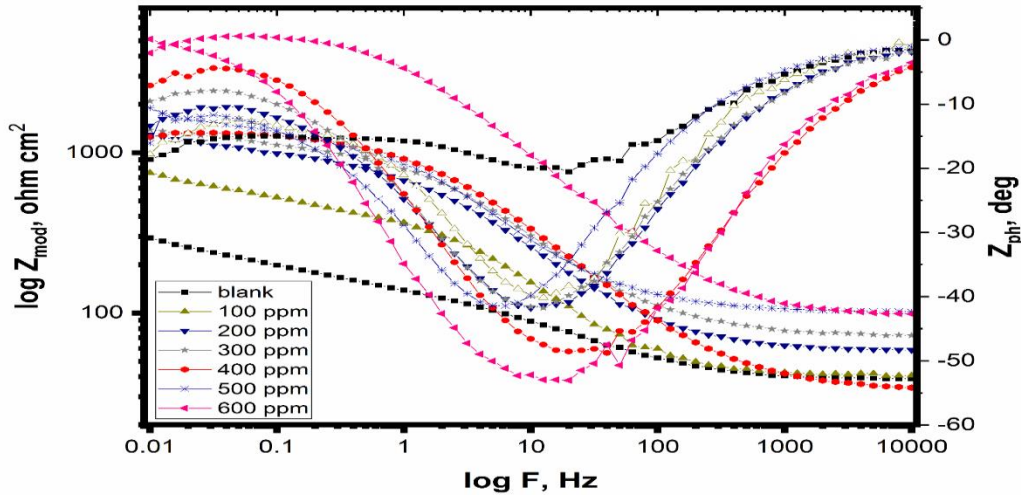

Fig. 11. Phase angle and Bode plots for Cu at 298 K without and with varying LFH concentrations.

The analogous circuit shown in Fig.12 was used to model and analyze the experimental results. Suitable R(Q(RW)) equivalent electrical circuit (EEC) with regard to Cu in SAR solution, either without or with LFH concentrations. The analogous circuit has two resistors: R_1, solution resistance (R_s), and R_2, the corrosion process' charge transfer resistance at Cu/solution interface, as well, W_2, the Warburg impedance caused by the diffusion of the corrosive reactant of the appropriate product species. In place of an ideal capacitance element, constant phase element (CPE) (Q_2) was developed to account for surface roughness and heterogeneities (El-Sayed et al., 2023a), and the following Equation describes the value for (CPE):

$$Z_{CPE} = Q_{dl}^{-1}(j\omega)^{-n} \tag{17}$$

In this equation, Q_{dl} represents CPE constant, ω represents angular frequency, j represents an imaginary number, and n represents CPE exponent as a function of surface inhomogeneity due

to inhibitor adsorption, surface roughness, and the formation of porous layers. When n is zero, Z_{CPE} is a resistance; when n is 1, Z_{CPE} is a capacitance; and when n is -1, Z_{CPE} is an inductance. In practice, an electrode's n value is often between zero and one. The rougher the electrode surface morphology is, the lower the value of n, suggesting severe electrode corrosion (Khaled et al., 2004).
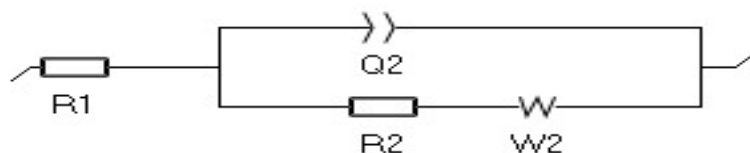

Fig. 12. Impedance data fitting equivalent circuit. Table 8 displays the differences in the copper's EIS parameters with and without LFH. Examination of Table 8 reveals that as LFH concentration rises, R_{ct} value rises while Q falls. The gradual substitution of H_2O molecules is likely responsible for the increase in both R_{ct} and the inhibition activity $\eta\%$ (Quartarone et al., 2008; Sherif et al., 2008) and hostile ions by adsorbing LFH molecules to a Cu surface, resulting in the formation of an adherent layer. Therefore, it is possible to infer that a reduction in double-layer thickness results from the produced film's increasing coverage of the copper substrate (Echihi et al., 2019; Tasić et al., 2018).

Additionally, it is noteworthy that the $\eta\%$ values inferred from the EIS interpretation and those acquired from WL and the potentiodynamic polarisation measurements reasonably agree.

Table 8. Variables of Cu impedance with different concentrations of LFH in SAR solution, as well as without LFH.

Conc. ppm	R_1 $k\Omega\ cm^2$	$Q-y^o$ $\mu\ \Omega^{-1}\ s^n\ cm^{-2}$	$Q-n$	R_{ct} $k\Omega\ cm^2$	W $\mu\Omega^{-1}\ s^{0.5}\ cm^{-1}$	θ	$\eta\%$
Blank	36.54	1524	0.53	0.157	26.63		
100	21.8	0.36	0.715	0.352	13	0.55	55.40
200	57.71	0.218	0.726	0.928	10	0.83	83.08
300	71.96	0.185	0.752	1.027	12.8	0.85	84.71
400	54.54	0.207	0.739	1.079	4.2	0.85	85.45
500	102.3	0.20	0.76	1.252	6.5	0.87	87.46
600	67.64	0.16	0.734	1.36	3.8	0.88	88.46

4. Surface morphology studies

Fig. (13a) demonstrates a Cu surface micrograph under 3500X magnification after being immersed in SAR solution for 6 hours without the drug; the same surface with 600 ppm of LFH is shown in Fig (13b), respectively. In free SAR solutions, the surface of the copper was massively deteriorated, and a large number of pits were observed (Fig. 13a). Fig. (13b) reveals that surfaces are almost free from damage, and they are smooth in the presence of 600 ppm of investigated drugs. This is probably because of the development of a protective adsorbed drug

layer on the copper surface, reducing metal corrosion. The results acquired by SEM analysis are generally in agreement with the behavior of copper in SAR solution in the absence and presence of the expired drugs shown by the potentiodynamic polarization and EIS experiments.

To explore the effect of LFH on the initiation and development of corrosion at the Cu/solution interface, (AFM) has emerged as a promising new method (Anbarasi et al., 2012; Sherine et al., 2010; Singh et al., 2011; Wang et al., 2011). AFM image analysis was used to determine the root mean square surface roughness (Sq) and mean roughness (Sa) for copper surfaces immersed in different environments. Table 9 summarizes Sq and Sa values for the Cu surface immersed in solution for SAR without and with LFH inhibitor. In Fig. 13a, the pitted, corroded metal surface was visible when immersed in SAR solution without the inhibitor; in this case, Sq and Sa values for the copper surface observed are 217.2 and 176.3 nm, respectively. Fig. 13b shows the copper surface after immersion in SAR containing 600 ppm of LFH. The values of Sq and Sa for the copper surface in the inhibited SAR solution are (151.4 and 118.2) for the LFH inhibitor. These parameters confirm the copper surfaces are smoother than the metal surface immersed in a blank SAR solution.

The aggregate structure generated at copper in the presence of pharmaceuticals is distinct from the corroded surface structure under uninhibited conditions (Fig. 13(a) and (b)). The difference is due to the drug molecules' spontaneous adsorption on the copper surface, where they formed an adsorbed coating that shielded the metal from further corrosion.
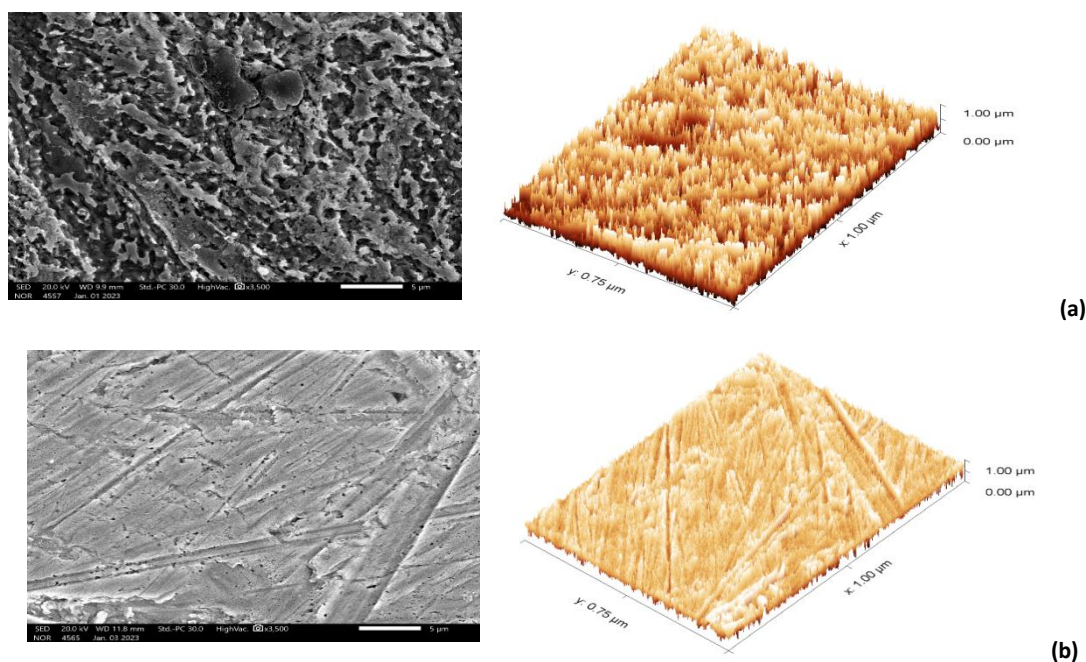

(a)

(b)

Fig. 13. Images of Cu SEM and AFM after immersion in (a) SAR and (b) SAR + LFH (600 ppm).

Montaser et al., 2024

Table 9. Copper surface AFM data for inhibited and uninhibited solutions.

Solution	Roughness, RMS (Sq), nm	Mean roughness (Sa), nm
SAR (blank)	217.2	176.3
SAR+ 600 LFH	151.4	118.2

Results from an EDX analysis show that LFH molecules adsorb onto the copper surface. In comparison to Fig. 14a, Fig. 14b reveals a lower fraction of oxygen atoms in copper oxides and a new peak for LFH carbon atoms. Table 10 displays the results of a comparison between copper surface immersed in inhibited and uninhibited solutions.

Fig. 14. Comparison of Cu surface EDX characteristics in SAR without (a) and
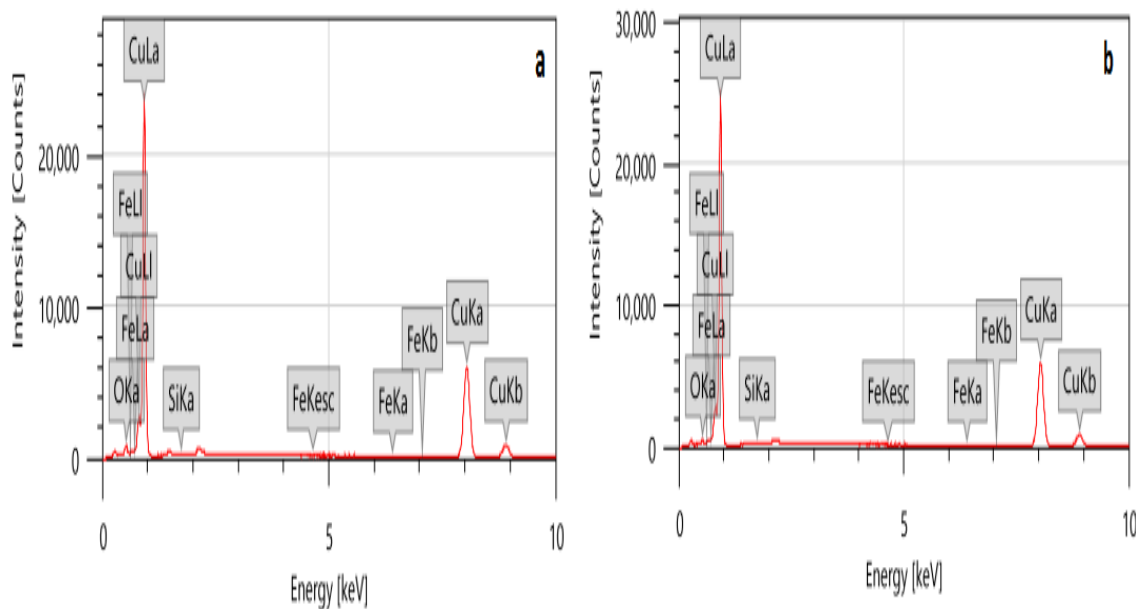
with LFH (b).

Table 10. Copper surface EDX data for inhibited and uninhibited solutions.

solution	C		O		Si		Fe		Cu	
	Mass %	Atom %	Mass %	Atom %	Mass %	Atom %	Mass %	Atom %	Mass %	Atom %
SAR	---	-----	2.11	7.90	0.05	0.1	0.08	0.08	97.76	91.92
SAR+600ppm LFH	4.08	17.98	0.78	2.59	0.78	2.59	0.04	0.07	94.98	79.19

4.3 FTIR Analysis

FTIR spectrum of pure LFH and its protective film after immersion in the SAR solution for 6 hours are shown in Fig. 15. FTIR spectra of pure LFH Fig. 15 (line a) shows a characteristic peak at 3360.5 cm^{-1}, which refers to the O–H stretching in COOH. The C=O stretching in COOH

and 4-quinolone ring were found at 1715.5 cm^{-1} and 1617.3 cm^{-1}, respectively. The peak at 1469.9 cm^{-1} suggested the C=C stretching in the aromatic ring. The peak at 1449.2 cm^{-1} was assigned to C–H bending, while the peak at 1340.1 cm^{-1} represented the C–N stretching which is attributed to the presence of the NH group. A strong absorption peak at 1106.5 cm^{-1} was assigned to the C–F group (Table 11). Fig. 15(line b) displays the FTIR spectrum of the protective coating generated on the Cu surface following immersion in SAR solution containing LFH for 6 hours. It was noticed that the O–H stretching has shifted from 3360.5 to 3352.2 cm^{-1}. The peak assigned to C=O in COOH stretching has shifted from 1715.5 to 1721.8. The bending vibration of the C-H group has shifted from 1449.2 to 1451.4 cm^{-1}. While the peaks of the C–N stretching have shifted from 1340.1 to 1342.1cm^{-1} (Table 11). Thus, the FTIR spectral study concludes that the LFH inhibitor adsorbed on the Cu surface.

Table 11. Pure LFH FTIR properties compared to those of an LFH-adsorbed film over a copper surface after 6 hours in SAR solution.

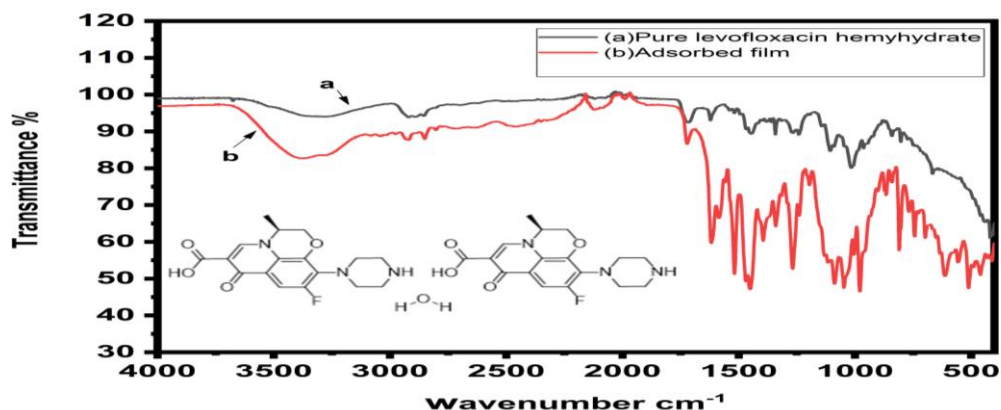| Group function	Pure LFH wavenumber, cm^{-1}.	Wavenumber of adsorbed film on a Cu surface, cm^{-1}.
O–H stretching in COOH	3360.5	3352.2
C=O stretching in COOH	1715.5	1721.8
4-quinolone ring stretching C=O	1617.3	1621.6
Aromatic ring C=C stretching	1469.9	1469.2
C–H bending	1449.2	1451.4
C–N stretching	1340.1	1342.1
Stretching C–O in COOH	1267.9	1269.3
Stretching C–F	1106.5	1108.8

Fig. 15. FTIR spectra of pure LFH drug (a) and its adsorbed film (b) on a Cu surface following six hours of immersion.

5. Mechanism of Corrosion Inhibition

Adsorption of LFH molecules on copper occurs because of the LFH molecules' transfer of electrons to Cu's vacant low-energy d orbitals. To prevent corrosion, an inhibitor's free electrons and/or π the electrons of aromatic rings must combine with an empty d orbital of the metal to form a donor-acceptor complex (Karthik et al., 2016). It's anticipated that LFH will favorably adsorb on the cathodic sites because It's a mixed-type inhibitor that mostly blocks the cathodic process, as shown by the polarisation curves.

Adsorption is affected by several factors, including the type of aggressive electrolyte, the nature and charge of the metal, as well as the inhibitor's chemical structure. Adsorption of organic inhibitors on metal surfaces often begins with the substitution of one or more water molecules already adsorbed there. Chemical and electrochemical studies imply mixed-inhibition mechanisms, which are in accordance with the literature (El Azhar et al., 2001; Oguzie et al., 2005) regarding the inhibitor molecule's adsorption behavior seen in Fig.16, which contains both N and O atoms.
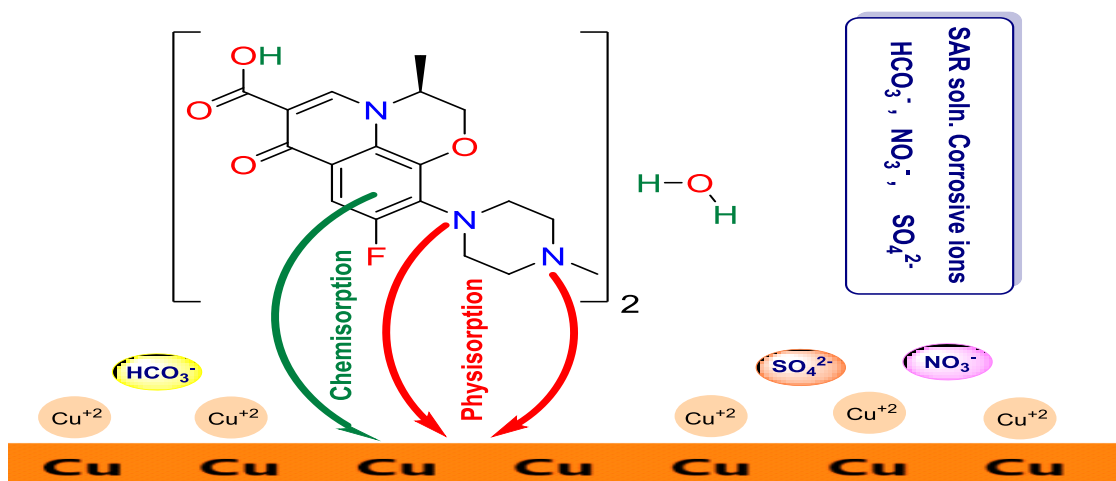

Fig. 16 Adsorption of LFH on Cu surface.

Copper corrosion in SAR solution has not been fully studied for its mechanism. Oxygen reduction is a well-known cathodic process in acidic media (Montaser et al., 2023). Cathodic redox reactions involve the reduction of oxygen and hydrogen that diffuse from the SAR solution and adsorb the surface of Cu:
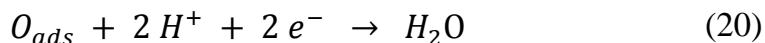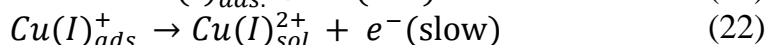
Hydrogen reduction:

$$2H^+ + 2e^- \rightarrow H_2 \qquad (18)$$

On the surface of the copper, oxygen diffuses from the bulk solution (Simonović et al., 2021; Žerjav et al., 2014):

$$O_{2,\ Bulk\ soln.} \rightarrow O_{2,\ Cu\ Surf.} \rightarrow O_{2,\ ads.} \qquad (19)$$
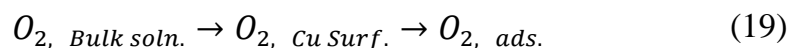
The next step is oxygen reduction, as indicated by the following Equation:

$$O_{ads} + 2H^+ + 2e^- \rightarrow H_2O \qquad (20)$$

Cu dissolution in acidic corrosive media is governed by the proposed mechanism (Jomy et al., 2022; Simonović et al., 2020):

$$Cu \rightarrow Cu(I)^+_{ads.} + e^- \text{(fast)} \qquad (21)$$
$$Cu(I)^+_{ads.} \rightarrow Cu(I)^{2+}_{sol.} + e^- \text{(slow)} \qquad (22)$$

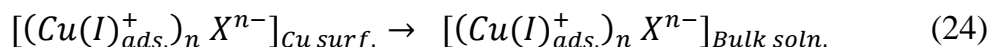As the anion X^{n-}_{bulk} diffuse onto the Cu surface from the SAR solution, $Cu(I)^+_{ads.}$ forms an association with it:

$$nCu(I)^+_{ads.} + X^{n-}_{Bulk} \rightarrow [(Cu(I)^+_{ads.})_n X^{n-}]_{surf} \qquad (23)$$
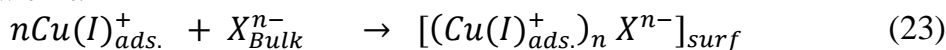
Then $(Cu(I)^+_{ads.})_n X^{n-}$ diffuses into the SAR solution:

$$[(Cu(I)^+_{ads.})_n X^{n-}]_{Cu\,surf.} \rightarrow [(Cu(I)^+_{ads.})_n X^{n-}]_{Bulk\,soln.} \qquad (24)$$

Therefore, it is reasonable to think of quasi-substitution between H_2O molecules on Cu surface ($H_2O_{ads.}$) and LFH compound in the aqueous phase (LHF_{sol}) during the adsorption of LFH molecules from aqueous solutions (El-Lateef et al., 2019; El-Sayed et al., 2023a) as represented in Equation (8). Thus, the inhibition mechanism on the Cu surface can be represented by the following reaction:

$$Cu + LFH_{ads.} \rightarrow [Cu - LFH_{ads.}] \qquad (25)$$

6. Conclusions

The following conclusion can be made on the basis of the foregoing findings.

1. According to the results, the medication LFH successfully prevents copper corrosion in the SAR solution. The η% of this compound rises as LFH concentrations rise and reaches its maximum value at 600 ppm concentration.

2. At various temperatures, the adsorption model follows the Langmuir isotherm. The inhibitor molecule adsorption is a spontaneous process, as indicated by the negative values of ΔG°_{ads}. In addition, an adsorption mechanism involves chemical (molecular) and physical (ionic) processes.

3. Based on polarisation curve analysis, the LFH was found to be a mixed-type inhibitor of Cu surface corrosion in SAR solution. Charge-transfer resistance is increased by the presence of LFH inhibitor, according to EIS plots, demonstrating that the performance of an inhibitor depends on the adsorption of molecules onto a metal surface. There is a fair amount of concordance between the weight loss, potentiodynamic polarization, and EIS approaches of inhibitory efficiency calculation.

4. Images from SEM and AFM confirm that a protective layer has developed on the copper surface.

References

Abd El Rehim, S. S., Hassan, H. H., & Amin, M. A. (2003). The corrosion inhibition study of sodium dodecyl benzene sulphonate to aluminium and its alloys in 1.0 M HCl solution. *Mater. Chem. Phys, 78*(2), 337-348. doi:https://doi.org/10.1016/S0254-0584(01)00602-2

Al-Bayaty, S. A., Jubier, N. J., & Al-Uqaily, R. A. H. (2020). Study of thermal decomposition behavior and kinetics of epoxy/polystyrene composites by using TGA and DSC. *Journal of Xian University of Architecture & Technology, 12*(3), 1331-1341. doi:https://doi.org/10.37896/jxat12.03%2F109

Al Kharafi, F. M., Al-Awadi, N. A., Ghayad, I. M., Abdullah, R. M., & Ibrahim, M. R. (2010). Novel technique for the application of azole corrosion inhibitors on copper surface. *Materials transactions, 51*(9), 1671-1676.

Anbarasi, M., & Rajendran, S. (2012). Surface Protection of Carbon Steel by Butanesulphonic Acid–Zinc Ion System. *Research Journal of Chemical Sciences, 2231*, 606X. doi:https://doi.org/10.1155/2014/628604

Aribou, Z., Ouakki, M., Khemmou, N., Sibous, S., Ech-chihbi, E., Benzekri, Z., . . . Touhami, M. E. (2023). Detailed experimental of indazole derivatives as corrosion inhibitor for brass in acidic environment: electrochemical/theoretical/surface studies. *Journal of Applied Electrochemistry*. doi:https://doi.org/10.1007/s10800-023-01960-6

Deng, S., Li, X., & Du, G. (2021). An efficient corrosion inhibitor of cassava starch graft copolymer for aluminum in phosphoric acid. *Chin. J. Chem. Eng, 37*, 222-231. doi:https://doi.org/10.1016/j.cjche.2020.08.013

Dueke‑Eze, C. U., Madueke, N. A., Iroha, N. B., Maduelosi, N. J., Nnanna, L. A., Anadebe, V. C., & Chokor, A. A. (2022). Adsorption and inhibition study of N-(5-methoxy-2-hydroxybenzylidene) isonicotinohydrazide Schiff base on copper corrosion in 3.5% NaCl. *Egyptian Journal of Petroleum, 31*(2), 31-37. doi:https://doi.org/10.1016/j.ejpe.2022.05.001

Echihi, S., Tabyaoui, M., & Qafsaoui, W. (2019). Inhibitive effect of 1, 3, 4-thiadiazole-2, 5-dithiol on copper corrosion in chloride media. *Int. J. Corros. Scale Inhib, 8*(2), 329-355. doi:http://dx.doi.org/10.17675/2305-6894-2019-8-2-14

El-Lateef, H. M. A., El-Sayed, A.-R., Mohran, H. S., & Shilkamy, H. A. S. (2019). Corrosion inhibition and adsorption behavior of phytic acid on Pb and Pb–In alloy surfaces in acidic chloride solution. *Int. J. Ind. Chem, 10*, 31-47. doi:https://doi.org/10.1007/s40090-019-0169-4

El-Sayed, A.-R., El-Hendawy, M. M., El-Mahdy, M. S., Hassan, F. S., & Mohamed, A. E. (2023a). The inhibitive action of 2-mercaptobenzothiazole on the porosity of corrosion film formed on aluminum and aluminum–titanium alloys in hydrochloric acid solution. *Sci. Rep, 13*(1), 4812. doi:https://doi.org/10.1038/s41598-023-31795-2

El-Sayed, A.-R., Mohamed, A. E., Hassan, F. S., & El-Mahdy, M. S. (2023b). Influence of Titanium Additions to Aluminum on the Microhardness Value and Electrochemical Behavior of Synthesized Aluminum-Titanium Alloy in Solutions of HCl and H3PO4. *J. Mater. Eng. Perform, 32*(4), 1760-1777. doi:https://doi.org/10.1007/s11665-022-07248-8

El-Sayed, N. S., & Kamel, S. (2022). Polysaccharides-Based Injectable Hydrogels: Preparation, Characteristics, and Biomedical Applications. *Colloids and Interfaces, 6*(4), 78. doi:https://doi.org/10.3390/colloids6040078

El Azhar, M., Mernari, B., Traisnel, M., Bentiss, F., & Lagrenée, M. (2001). Corrosion inhibition of mild steel by the new class of inhibitors [2,5-bis(n-pyridyl)-1,3,4-thiadiazoles] in acidic media. *Corrosion Science, 43*(12), 2229-2238. doi:https://doi.org/10.1016/S0010-938X(01)00034-8

El Ibrahimi, B. (2021). Sustainable Corrosion Inhibitors for Copper and its Alloys. *Sustainable Corrosion Inhibitors, 107*, 175. doi:https://doi.org/10.21741/9781644901496-7

Fan, G., Liu, H., Fan, B., Ma, Y., Hao, H., & Yang, B. (2020). Trazodone as an efficient corrosion inhibitor for carbon steel in acidic and neutral chloride-containing media: Facile

synthesis, experimental and theoretical evaluations. *Journal of Molecular Liquids, 311*, 113302. doi:https://doi.org/10.1016/j.molliq.2020.113302

Farag, A. A., & Hegazy, M. A. (2013). Synergistic inhibition effect of potassium iodide and novel Schiff bases on X65 steel corrosion in 0.5 M H2SO4. *Corrosion Science, 74*, 168-177. doi:https://doi.org/10.1016/j.corsci.2013.04.039

Fateh, A., Aliofkhazraei, M., & Rezvanian, A. (2020). Review of corrosive environments for copper and its corrosion inhibitors. *Arab. J. Chem, 13*(1), 481-544. doi:https://doi.org/10.1016/j.arabjc.2017.05.021

Fouda, A., Khalil, E., El-Mahdy, G., Shaban, M., Mohammed, A., & Abdelsatar, N. (2023). Synthesis and characterization of novel acrylamide derivatives and their use as corrosion inhibitors for carbon steel in hydrochloric acid solution. *Sci. Rep, 13*(1), 3519. doi:https://doi.org/10.1038/s41598-023-30574-3

Fouda, A. E., El-Dossoki, F., Hamed, E., & El-Hossiany, A. (2022). Inhibition Efficiency of Erdosteine Drug for 304L Stainless Steel Corrosion and Its Solvation Thermodynamic Parameters. *Egypt. J. Chem, 65*(13), 455-475. doi:https://doi.org/10.21608/EJCHEM.2022.131748.5806

Ikpi, M., Abeng, F., & Okonkwo, B. (2017a). Experimental and computational study of levofloxacin as corrosion inhibitor for carbon steel in acidic media. *WNOFNS*(9), 79-90.

Ikpi, M. E., & Abeng, F. E. (2017b). Electrochemical impedance spectroscopy and gravimetric study of the corrosion inhibition of API 5L X-52 steel in HCl medium by levofloxacin. *Int. J. Sci. Res, 6*, 623-628. doi:https://doi.org/10.21275/7071704

Jomy, J., Sharma, S., Prabhu, P., & Prabhu, D. (2022). Corrosion Behavior of EN18 Steel and Copper in the Sulfuric Acid Medium for As-Bought and Annealed Materials. *J. Mater. Eng. Perform*, 1-15. doi:https://doi.org/10.1007/s11665-022-07698-0

Karthik, G., & Sundaravadivelu, M. (2016). Investigations of the inhibition of copper corrosion in nitric acid solutions by levetiracetam drug. *Egyptian Journal of Petroleum, 25*(4), 481-493. doi:https://doi.org/10.1016/j.ejpe.2015.10.009

Khaled, K., & Hackerman, N. (2004). Ortho-substituted anilines to inhibit copper corrosion in aerated 0.5 M hydrochloric acid. *Electrochim. Acta, 49*(3), 485-495. doi:https://doi.org/10.1016/j.electacta.2003.09.005

Kuraimid, Z. K., Abid, D. S., & Fouda, A. A. S. (2023). Insight into the use of 1, 3, 5, 7-tetrahexyl-1, 3, 5, 7-tetraazaadamantane-1, 3, 5, 7-tetraium bromide as a highly efficient inhibitor for the corrosion of C1018 low-carbon steel in acidic medium: Synthesis, characterization, and electrochemical studies. *Int. J. Corros. Scale Inhib, 12*(3), 984-1001.

Lamaka, S. V., Zheludkevich, M. L., Yasakau, K. A., Serra, R., Poznyak, S., & Ferreira, M. (2007). Nanoporous titania interlayer as reservoir of corrosion inhibitors for coatings with self-healing ability. *Prog. Org. Coat, 58*(2-3), 127-135. doi:https://doi.org/10.1016/j.porgcoat.2006.08.029

Li, C.-c., Guo, X.-y., Shen, S., Song, P., Xu, T., Wen, Y., & Yang, H.-F. (2014). Adsorption and corrosion inhibition of phytic acid calcium on the copper surface in 3 wt% NaCl solution. *Corrosion Science, 83*, 147-154. doi:https://doi.org/10.1016/j.corsci.2014.02.001

Lyon, R. C., Taylor, J. S., Porter, D. A., Prasanna, H. R., & Hussain, A. (2006). Stability profiles of drug products extended beyond labeled expiration dates. *J. Pharm. Sci, 95 7*, 1549-1560. doi:https://doi.org/10.1002/jps.20636

Montaser, A. A., El-Mahdy, M. S., Mahmoud, E. E. E., & Fouda, A. S. (2023). Recycling of expired ciprofloxacin in synthetic acid rain (SAR) solution as a green corrosion inhibitor for copper: a theoretical and experimental evaluation. *Journal of Applied Electrochemistry*. doi:10.1007/s10800-023-01966-0

Mu, G., & Li, X. (2005a). Tween-40 as corrosion inhibitor for cold rolled steel in sulphuric acid: weight loss study, electrochemical characterization, and AFM. *Appl. Surf. Sci., 252*, 1254-1265. doi:https://doi.org/10.1016/j.apsusc.2005.02.118

Mu, G., Li, X., & Liu, G. (2005b). Synergistic inhibition between tween 60 and NaCl on the corrosion of cold rolled steel in 0.5M sulfuric acid. *Corrosion Science, 47*(8), 1932-1952. doi:https://doi.org/10.1016/j.corsci.2004.09.020

Oguzie, E. E., Onuoha, G. N., & Onuchukwu, A. I. (2005). Inhibitory mechanism of mild steel corrosion in 2M sulphuric acid solution by methylene blue dye. *Materials Chemistry and Physics, 89*(2), 305-311. doi:https://doi.org/10.1016/j.matchemphys.2004.09.004

Pang, X.-H., Zhang, Y.-X., Zhang, J., Jie, J.-D., & Hou, B.-R. (2011). Corrosion inhibition and mechanisms study on pipemidic acid, levofloxacin and ciprofloxacin for mild steel in 0.5 mol/L H2SO4. *Acta Chimica Sinica, 69*(04), 483.

Quartarone, G., Battilana, M., Bonaldo, L., & Tortato, T. (2008). Investigation of the inhibition effect of indole-3-carboxylic acid on the copper corrosion in 0.5 M H2SO4. *Corrosion Science, 50*(12), 3467-3474. doi:https://doi.org/10.1016/j.corsci.2008.09.032

Rajeswari, V., Devarayan, K., & Viswanathamurthi, P. (2017). Expired pharmaceutical compounds as potential inhibitors for cast iron corrosion in acidic medium. *Res. Chem. Intermed, 43*, 3893-3913. doi:https://doi.org/10.1007/s11164-016-2852-9

Raviprabha, K., Bhat, R. S., Bhat, S. I., Nagaraj, P., & Jyothi, K. (2023). Corrosion inhibition study of 6061 aluminium alloy in the presence of ethyl 5-methyl-1-(4-nitrophenyl)-1H-1,2,3-triazole-4-carboxylate (NTE) in hydrochloric acid. *Heliyon, 9*(5), e16036. doi:https://doi.org/10.1016/j.heliyon.2023.e16036

RAZLI, K. S., & UMETNEM, N. B. V. (2011). Corrosion stability of different bronzes in simulated Urban rain. *Mater. Tehnol, 45*(6), 585-591.

Sherif, E.-S. M., Erasmus, R., & Comins, J. (2008). Inhibition of copper corrosion in acidic chloride pickling solutions by 5-(3-aminophenyl)-tetrazole as a corrosion inhibitor. *Corrosion Science, 50*(12), 3439-3445. doi:https://doi.org/10.1016/j.corsci.2008.10.002

Sherine, B., Nasser, A. A., & Rajendran, S. (2010). Inhibitive action of hydroquinone-Zn2+ system in controlling the corrosion of carbon steel in well water. *IJEST, 2*(4), 341-357.

Simonović, A., Mihajlović, M. P., Radovanović, M., Tasić, Ž., & Antonijević, M. (2021). Inhibition of Copper Corrosion in Acid Rain Solution Using the Imidazole Derivatives. *Russian Journal of Electrochemistry, 57*(5), 544-553. doi:http://dx.doi.org/10.1134/S102319352012023X

Simonović, A. T., Tasić, Z. a. Z., Radovanović, M. B., Petrović Mihajlović, M. B., & Antonijević, M. M. (2020). Influence of 5-chlorobenzotriazole on inhibition of copper corrosion in acid rain solution. *ACS omega, 5*(22), 12832-12841. doi:https://doi.org/10.1021/acsomega.0c00553

Singh, A. K., & Quraishi, M. (2011). Investigation of the effect of disulfiram on corrosion of mild steel in hydrochloric acid solution. *Corrosion Science, 53*(4), 1288-1297. doi:https://doi.org/10.1016/j.corsci.2011.01.002

Singh, P., Chauhan, D. S., Srivastava, K., Srivastava, V., & Quraishi, M. A. (2017). Expired atorvastatin drug as corrosion inhibitor for mild steel in hydrochloric acid solution. *Int. J. Ind. Chem, 8*(4), 363-372. doi:https://doi.org/10.1007/s40090-017-0120-5

Tasić, Ž. Z., Mihajlović, M. B. P., Radovanović, M. B., Simonović, A. T., & Antonijević, M. M. (2018). Cephradine as corrosion inhibitor for copper in 0.9% NaCl solution. *J. Mol. Struct, 1159*, 46-54. doi:https://doi.org/10.1016/j.molstruc.2018.01.031

Tasić, Z. Z., Mihajlović, M. B. P., Simonović, A. T., Radovanović, M. B., & Antonijević, M. M. (2019). Ibuprofen as a corrosion inhibitor for copper in synthetic acid rain solution. *Sci. Rep, 9*(1), 14710. doi:https://doi.org/10.1038/s41598-019-51299-2

Thanapackiam, P., Mallaiya, K., Rameshkumar, S., & Subramanian, S. S. (2017). Inhibition of corrosion of copper in acids by norfloxacin. *Anti-Corrosion Methods and Materials, 64*(1), 92-102. doi:http://dx.doi.org/10.1108/ACMM-12-2015-1617

Thanapackiama, P., Subramaniama, E. P., Hemalathaa, K. V., & Gayathria, B. (2019). Electrochemical study of inhibition of corrosion of copper by ofloxacin in acid media. *J. Environ. Nanotechnol, 8*(1), 75-88. doi:doi: 10.13074/jent.2019.03.191349.

Varvara, S., Damian, G., Bostan, R., & Popa, M. (2022). Inhibition effect of Tantum Rosa drug on the corrosion of copper in 3.5 wt.% NaCl solution. *International Journal of Electrochemical Science, 17*(9), 220958. doi:https://doi.org/10.20964/2022.09.56

Wang, B., Du, M., Zhang, J., & Gao, C. (2011). Electrochemical and surface analysis studies on corrosion inhibition of Q235 steel by imidazoline derivative against CO2 corrosion. *Corrosion Science, 53*(1), 353-361. doi:https://doi.org/10.1016/j.corsci.2010.09.042

Xu, S., Luo, Z., Zhang, J., Tan, B., Zhang, S., & Li, W. (2021). Study on corrosion inhibition performance of 1-dodecyl-3-methyl-1 h-imidazolium nitrate on Cu in the sulfuric acid environment. *Journal of Molecular Liquids, 340*, 117189. doi:https://doi.org/10.1016/j.molliq.2021.117189

Yao, J., & Trokourey, A. (2019). Thermodynamic and DFT studies on the behavior of cefadroxil drug as effective corrosion inhibitor of copper in one molar nitric acid medium. *J Mater Environ Sci, 10*, 926-938.

Zarrouk, A., Hammouti, B., Zarrok, H., Al-Deyab, S., & Messali, M. (2011). Temperature effect, activation energies and thermodynamic adsorption studies of L-cysteine methyl ester hydrochloride as copper corrosion inhibitor in nitric acid 2M. *Int. J. Electrochem. Sci, 6*(12), 6261-6274. doi:https://doi.org/10.1016/S1452-3981(23)19679-9

Žerjav, G., & Milošev, I. (2014). Carboxylic acids as corrosion inhibitors for Cu, Zn and brasses in simulated urban rain. *Int. J. Electrochem. Sci, 9*(5), 2696-2715. doi:https://doi.org/10.1016/S1452-3981(23)07957-9

Zhang, Q., Zhu, Z., Liu, P., Zhang, J., & Cao, F. (2019). Corrosion electrochemical kinetic study of copper in acidic solution using scanning electrochemical microscopy. *Journal of The Electrochemical Society, 166*(13), C401. doi:https://doi.org/10.1149/2.0061913jes

Zheng, T., Wang, L., & Liu, J. (2020). Corrosion inhibition of levofloxacin and Ce(NO3)3 for AA2024-T4 in 3.5% NaCl. *Corros. Eng. Sci. Technol, 55*(1), 75-82. doi:https://doi.org/10.1080/1478422X.2019.1681152